Hysteresis and drift of spiral waves near heterogeneities: From chemical experiments to cardiac simulations

Elias Nakouzi, Jan Frederik Totz, Zhihui Zhang, Oliver Steinbock, and Harald Engel

Phys. Rev. E **93**, 022203 — Published 4 February 2016

DOI: 10.1103/PhysRevE.93.022203

Hysteresis and Drift of Spiral Waves Near Heterogeneities: From Chemical Experiments to Cardiac Simulations

Elias Nakouzi, Jan Frederik Totz[†], Zhihui Zhang, Oliver Steinbock, and Harald Engel[†*]

Florida State University, Department of Chemistry and Biochemistry, Tallahassee, FL 32306-4390 and

[†]*Institut für Theoretische Physik, Technische Universität Berlin, Hardenbergstraße 36, 10623 Berlin, Germany*

(Dated: Nov. 24, 2015)

Abstract

Dissipative patterns in excitable reaction-diffusion systems can be strongly affected by spatial heterogeneities. Using the photosensitive Belousov-Zhabotinsky reaction, we show a hysteresis effect in the transition between free and pinned spiral rotation. The latter state involves the rotation around a disk-shaped obstacle with an impermeable and inert boundary. The transition is controlled by changes in light intensity. For permeable heterogeneities of higher excitability, we observe spiral drift along both linear and circular boundaries. Our results confirm recent theoretical predictions and, in the case of spiral drift, are further reproduced by numerical simulations with a modified Oregonator model. Additional simulations with a cardiac model show that orbital motion can also exist in anisotropic and three-dimensional systems.

PACS numbers: 05.45.-a, 82.40.Ck, 82.40.Qt

* Corresponding author; harald.engel@tu-berlin.de

I. INTRODUCTION

In excitable systems far from equilibrium, macroscopic structures can spontaneously self-organize. This pattern formation and in particular propagating waves in reaction-diffusion media have attracted interest across a broad range of disciplines. Examples include adsorption patterns in the oxidation of CO on platinum surfaces [1, 2], action potentials in cardiac tissue [3, 4], and messenger signals in social amoebae [5, 6]. More recently, there has also been evidence for nonlinear wave processes controlling the contractions of the human uterus during labor [7].

The Belousov-Zhabotinsky (BZ) reaction presents an excellent model for studying excitation waves in reaction-diffusion systems [8, 9]. In spatially two-dimensional media, these chemical waves can evolve into rotating spirals which have a characteristic rotation period (T) and wavelength (λ). The spiral tip is a non-stationary phase singularity acting as the pacemaker for the rotating vortex. In the simplest case, the tip rigidly rotates in a circular orbit that defines the core radius. Alternatively, the tip trajectory describes "meandering" paths such as hypotrochoidal or epitrochoidal curves.

An interesting variant of the BZ reaction utilizes the photosensitive ruthenium-bipyridyl complex as the redox catalyst [10, 11]. In this system, external light sources can be used to photochemically excite the complex which then enhances the production of inhibitory Br^- ions. Accordingly, an increase in light intensity causes a decrease in the excitability of the reaction medium, which also results in altered and typically more expansive tip trajectories. These photo-induced changes allow for the fast, local or global, perturbation of the excitation waves. It is hence no surprise that numerous studies have utilized this reaction to analyze excitable and oscillatory systems under periodic forcing and feedback [10, 14, 15]. Such perturbations can induce spiral wave drift that has been used to actively reposition spiral cores. Spiral wave drift also occurs in response to external perturbations such as externally applied electric fields [16], parameter gradients [17], nearby Neumann boundaries [18], and other spirals [12, 19].

Several studies have investigated the interaction of rotating vortices with spatial heterogeneities from an experimental [12, 20–24] and theoretical perspective [25–28]. Unexcitable obstacles can pin spiral waves thus confining their tip motion to the perimeter of the anchoring site. This effect is particularly relevant to reentrant waves in cardiac muscle which form

pinned states at tissue heterogeneities [29–31]. Ventricular fibrillation can occur when these pinned vortices devolve into a turbulent state. Recent studies have reported the resetting of cardiac activity by repeatedly applying electric shocks of low power [32, 33].

In this Article, we experimentally validate two recent theoretical predictions on spiral wave dynamics in the presence of heterogeneities. The first set of experiments examines the hysteresis in the transition of spirals between pinned and unpinned states. In a numerical study, Zykov et al. predicted this effect for spiral waves rotating around circular, impermeable obstacles [26]. The angular velocity of the spiral tip (ω) shows a bistability as the obstacle radius (r_h) is varied. At a given r_h, the value of ω for a pinned spiral is different than for the corresponding free spiral, thus suggesting a hysteresis effect. In the second set of experiments, we investigate spiral drift induced by a localized heterogeneity in the reaction medium. Using asymptotic theory, Biktashev et al. predicted the existence of orbitals of alternating stability around the heterogeneity [27]. For the case of a circular heterogeneity of higher excitability, the spiral wave performs an orbital motion of constant radius. Lastly, we compare our experimental results to numerical simulations using a modified Oregonator and a three-dimensional cardiac model.

II. EXPERIMENTAL METHODS

Our experiments are conducted in a flow reactor using the photosensitive ruthenium-catalyzed Belousov-Zhabotinsky (BZ) reaction. We prepare the BZ system as described by Kheowan et al. [13] with minor modifications. The reactant concentrations are [$NaBrO_3$] = 0.20 mol/L, [H_2SO_4] = 0.39 mol/L, [malonic acid] = 0.17 mol/L, and [NaBr] = 0.09 mol/L. To minimize 3D effects, the reaction is confined to a thin hydrogel layer. For this purpose, a catalyst-gel solution is prepared by mixing 2.6 mL of 15% $Na_2(SiO_2)_3O$, 0.076 mL of 3×10^{-2} mol/L of ruthenium-4,4'-dimethyl-2,2'-bipyridyl chloride further abbreviated $Ru(dmbpy)_3Cl_2$, 0.6 mL of 1 mol/L H_2SO_4, and 2.42 mL of distilled water. An approximately 1.15 mL aliquot of this pregel solution is spread on a glass plate of diameter 7 cm yielding a 0.40 $\pm$ 0.1 mm thick layer containing the catalyst at a concentration [$Ru(dmbpy)_3{}^{2+}$] = 2.4×10^{-3} mol/L. For the experiments in which an impermeable heterogeneity is required, a small glass disk of radius 0.65 mm is inserted in the gel during preparation. It is important that the disk height is comparable to the gel thickness in

order to avoid surface tension effects. We also attempted other methods for creating the obstacle such as mechanical removal and laser ablation of a gel piece but this approach causes unwanted, permanent deformations around the excision site [34].

After preparation, the glass plate supporting the hydrogel matrix is fixed firmly in the reactor using a rubber O-ring. The reactor is then filled with 100 mL of the catalyst-free BZ solution which is stirred at a constant rate. Notice that the reaction occurs almost exclusively in the gel matrix which contains the catalyst component. A peristaltic pump continuously delivers fresh solution and discharges the product species. This setup creates a transient-free condition far from equilibrium that is only perturbed by a slow loss of catalyst, which we further minimize by the use of the 4,4'-dimethyl-2,2'-bipyridyl ligand in our catalyst [12]. Furthermore, a fresh hydrogel sample is prepared for each experimental run. The reaction medium is maintained at 22°C by pumping water through the reactor jacket.

The experimental setup is illustrated in Fig. 1. The observation light source is a blue LED (maximum emission at 460 nm) equipped with a yellow, long-pass filter (Edmund Optics, GG-475). This combination yields good visual contrast between the oxidized and the reduced catalyst species while minimizing the influence of the observation light on the catalyst behavior. The light is passed through a condenser lens and then through the BZ reactor. A beam splitter (30R/70T, Edmund Optics, NT 46-632) redirects a portion of the transmitted light to a charge-coupled device camera (Imaging Source Europe, DMK 41BU02.H) which collects image data at 1 s intervals. The CCD camera is connected to a computer and data acquisition is performed using LabVIEW software [34]. A separate LED lamp (Casio XJ A140V, 2500 ANSI Lumens) equipped with a blue, dichroic filter (Edmund Optics, NT30-635) is used for illumination of the working area. Higher light intensity of around 452 nm induces photo-excitation of $Ru(dmbpy)_3^{2+}$ and thus inhibits the BZ reaction. The light intensity of the projector is controlled via LabVIEW, which effectively allows the modification of the global excitability of the reaction medium. In addition, a spatially defined light intensity profile can be applied, which produces a reaction medium with non-homogeneous excitability. Note that the wavelengths of the static observation and the controlled light sources overlap to some extent. Accordingly, the light intensities are reported relative to the maximum controlled light intensity in every set of experiments.

To initiate a spiral wave, a light spot of high intensity is created transiently on a spontaneously formed wavefront. This erases the illuminated portion of the propagating wave and

allows the open ends of the wavefront to curl inwards and evolve into a spiral wave pair. To obtain a spiral wave pinned to an unexcitable obstacle, the broken wavefront should be in contact with the obstacle disk. In-house programs are incorporated in the LabVIEW platform to provide real time measurement of the wave period and the tip location. The latter is detected as the intersection of isocontours in successive grayscale images.

III. EXPERIMENTAL RESULTS

We first investigate the dynamics of spiral waves rotating around an unexcitable and impermeable heterogeneity. Figures 2(a,b) show experimental images of a spiral wave in the thin gel layer of our chemical reactor. Image contrast results from variations in the concentration ratio of the oxidized and the reduced catalyst which have different absorption spectra. Accordingly, bright and dark areas correspond to regions with high concentrations of $[Ru(dmbpy)_3]^{3+}$ and $[Ru(dmbpy)_3]^{2+}$, respectively. Embedded in the gel is a small glass disk that can be discerned as a bright spot near the center of the images. The radius of the disk is 0.65 mm which compares roughly to 15% of the spiral wavelength (λ). In Figure 2(a) the spiral tip is pinned to this heterogeneity and steadily revolves around it. In Figure 2(b), however, the spiral is not attached to the disk and, at this particular instance, the distance between the tip and the disk equals nearly one wavelength of the spiral. In the following, we refer to these two different cases as the pinned and the unpinned (or free) state.

The two states shown in Fig. 2 occur at different global light intensities. Specifically, the light intensity in Fig. 2(a) is approximately 14% lower than in Fig. 2(b). While it is obviously always possible for a spiral to be unpinned, pinning occurs only at low light intensities. In Fig. 3, we characterize the response of spiral waves to a slow, sawtooth-shaped variation in light intensity [35]. More precisely, we adjust the intensity in small steps that occur whenever the tip has completed a full rotation. The typical experiment commences with a pinned spiral. At a critical intensity, the tip detaches from the heterogeneity and describes a nearly circular orbit. This orbit is 2.7 times larger than the inert disk and corresponds to the most expansive trajectory in Fig. 3(a) (solid, black circles). Subsequently, we reduce the light intensity and observe a steady decrease in the size of the circular, unpinned orbits (blue markers in Fig. 3(a)). These trajectories touch the heterogeneity because a reduction in the size of the orbit must necessarily induce a collision between the

tip and the disk. Eventually, the light intensity has decreased sufficiently and the spiral re-pins.

Figure 3(b) shows an analysis of the latter dynamics by plotting the radius of the tip orbit r as a function of the applied light intensity P. The ordinate is rescaled in terms of the wavelength (pitch) of the pinned spiral ($\lambda_p = 3.85$ mm). Solid and open markers distinguish values measured for increasing and decreasing light intensities, respectively. The data are obtained from one, representative experiment. Initially, the spiral wave is pinned to the obstacle and r is equivalent to the radius of the heterogeneity (r_h) which equals approximately 0.17λ. For increasing light intensities, the spiral wave retains the same r as long as it is in the pinned state (solid, red markers). At the critical intensity (here set to $P = 1$ a.u.), the spiral wave unpins from the anchoring disk and r increases abruptly to 0.49λ (open, black marker). During the subsequent decrease in P, the spiral remains unpinned at decreasing r values, although earlier the same intensities yielded stable pinning (open, blue markers). The pinned state is re-established only when P has reached a value close to 0.9 a.u. We emphasize that the light intensity required for unpinning the anchored spiral is larger than that required to pin the free vortex. Clearly the transition between the two states can be interpreted as hysteresis.

As further evidence of the hysteresis effect, we analyze the change in the period, or more precisely the interpulse time, within the spiral wave pattern. Figure 4 graphs the variation in image contrast at an arbitrary, constant point in the reaction medium. Each peak corresponds to a propagating wave pulse passing through this site. The period is measured as the time elapsed between two consecutive intensity maxima. At the start of the experiment, the pinned spiral has a period of $T = 80 \pm 3$ s. This value increases only slightly as the light intensity is increased as long as the spiral wave is in the pinned state (solid, red curve). After the unpinning event at $P = 1$ a.u., the period increases substantially (dashed, blue curve) to $T = 257$ s. This result is consistent with our observation that the released spiral has a significantly larger value of r and by extension a larger period. The period then decreases gradually as the applied light intensity is decreased, thus resembling the observed trend in r. Note that the black arrows in Fig. 4 correspond to these changes in applied light intensity as described earlier. Finally, a value close to the original period is recovered after the spiral returns to the pinned state (solid, red curve). The 16% increase in the period between the re-pinned spiral and the initial value is ascribed to the slow transients in our

chemical reactor, which are predominantly caused by the loss of catalyst from the gel into the flowing solution. We also note that the times between the intensity peaks are not exact representations of the rotation periods at fixed light intensities because such measurements would require longer time intervals between the applied intensity changes. Such longer experiments, however, would amplify the impact of the aforementioned transients in the reactor system and are hence problematic.

The hysteresis phenomenon established by the results in Figs. 3 and 4 is closely related to recent theoretical results by Zykov et al. [26]. Using the FitzHugh-Nagumo model and continuation methods, these authors studied the pinning/unpinning transition by varying the radius of the pinning site (r_h). Their results show hysteresis over a range of r_h values and qualitatively similar changes in the rotation period. Clearly, varying the size of a disk with a no-flux boundary is experimentally challenging. However, we attempted to test these predictions in our experiments by creating a spot of high illumination intensity, which generates an unexcitable disk but does not surround this disk with a no-flux boundary. As expected from earlier studies, this method can indeed pin the spiral wave and readily allows the variation of the disk radius [36]. The hysteresis effect, however, could not be observed with this experimental approach. This negative result suggests that a no-flux boundary is necessary for the described hysteresis effect.

In a second set of experiments, we study the behavior of spiral waves in the presence of heterogeneities of higher excitability that are either large regions with straight borders or small disks [35]. The former case is illustrated in Fig. 5. The dashed, red line indicates the border between the right-side region of high excitability and left-side region of low excitability (Fig. 5(a)). To produce this transition line, we project a corresponding illumination pattern onto the system for which the light intensity varies by 20% in a step-like fashion. The spiral tip resides in the less excitable, region to the left. Notice that the width of the wave pulses varies slightly between the two regions as a direct consequence of the applied pattern of photo-inhibition. Along the border line, we observe deformations of the wavefronts, which are caused by differences in the wave velocity. These deformations are small near the spiral tip but increase with increasing distances from the wave source. The latter effect has been analyzed earlier using kinematic models and a generalized refractive

index [37, 38].

The experimental situation in Fig. 5(a) gives rise to a steady, linear drift of the spiral wave. Figure 5(b) shows the resulting tip trajectory for a representative experiment. In these measurements, we first allow the spiral to establish a steady rotation pattern. During this phase, the system is homogeneously illuminated at an intensity that corresponds to the subsequent condition of low excitability. We then create the darker area in close vicinity (less than one pattern wavelength) of the spiral tip. In response, the tip is transiently attracted to the dark heterogeneity and then drifts parallel to the border describing the curve shown in Fig. 5(b). Notice that the trajectory does not enter the dark region of higher excitability. Furthermore, the trajectory is well described by a prolate cycloid and, in the context of the figure, extends in a downward direction. In our experiments, this direction is characteristic of counter-clockwise rotating spirals whereas clockwise rotating vortices drift upwards. We find that the average drift velocity is fairly constant over the course of the individual experiments and preliminary measurements suggest that this speed increases with increasing intensity differences between the two regions.

Figure 6(a) shows a snapshot of a spiral wave in the vicinity of a circular light heterogeneity. The dashed, red circle represents the region of 20% lower light intensity. The corresponding spiral motion shown in Fig. 6(b) can be understood qualitatively in terms of periodic changes in the curvature of the tip trajectory. When the spiral tip is close to the dark heterogeneity, it turns at a faster rate since the recovery time of the reaction medium is shorter. In contrast, the tip rotation is slower when the spiral is turning deeper into the less excitable, bright region. The net result is an inhomogeneity-induced drift of the tip along the border which occurs at a constant distance to the dark region and at a constant average speed. Furthermore, it accounts for our observation of a chirality-dependent drift direction. We note that this explanation is related to the mechanism generating "petals" and "arcs" in the tip trajectories of meandering or externally entrained spirals [10]. The main discrepancy is that in the latter cases the spatial gradient in the recovery time is not forced by a static heterogeneity in the system but rather by the spiral wave itself or a time-dependent, external modulation.

Recently Biktashev et al. reported theoretical results on the interaction of spiral waves with localized heterogeneities [27]. They predict the existence of stationary orbits of alternating stability around a circular heterogeneity. In the case of a disk-shaped heterogeneity

with an increased excitability, the spiral tips experience a repulsion force at a small distance and an attraction force at a large distance and are hence forced to perform a stable orbital motion of constant radius. Our experiments with disk-shaped heterogeneities validate this prediction. Specifically, Fig. 6(b) shows that the spiral tip indeed embarks on a heterogeneity-induced orbital motion. Since stable orbits beyond the innermost one offer only weak attractive forces, we speculate that the initial portion of the tip trajectory in Fig. 6(b) follows the first stable orbit. After completing half of a rotation, however, the tip drifts away from the circular orbit, which we ascribe to unwanted gradients in the intended illumination pattern.

IV. OREGONATOR SIMULATIONS

Our experimental results agree with recently reported theoretical predictions of spiral wave dynamics near heterogeneities [26, 27]. However, the computational results in these studies were obtained for models that are not based on mass-action reaction mechanisms. We therefore perform additional simulations using a modified three-component Oregonator model [19, 39]. This model is derived from the Field-Körös-Noyes mechanism [40] of the BZ reaction and explicitly accounts for the rescaled concentrations of the activator $HBrO_2$ (u), the oxidized catalyst (v), and the inhibitor Br^- (w) :

$$\frac{\partial u}{\partial t} = \frac{1}{\epsilon_u}[u(1-u) + w(q-u)] + D_u \nabla^2 u, \tag{1a}$$

$$\frac{\partial v}{\partial t} = u - v, \tag{1b}$$

$$\frac{\partial w}{\partial t} = \frac{1}{\epsilon_w}[\phi - w(q+u) + fv] + D_w \nabla^2 w. \tag{1c}$$

The parameter ϕ models the photo-inhibition in the ruthenium-catalyzed BZ system and is analogous to the intensity of the externally applied illumination [39]. Notice that the diffusion term is omitted in Eq. (1b) because in our experiments, the catalyst is essentially immobilized within the thin gel layer. In all simulations, we use the following parameter values: $\epsilon_u = 0.0699$, $\epsilon_w = 2.78\times10^{-4}$, $q = 0.002$, $f = 1.4$, $D_u = 1.0$, $D_w = 1.2$, and $\phi = 0.035$. This parameter set induces excitable dynamics and spiral tips follow circular trajectories. The model equations are integrated numerically using the forward Euler method and a time step of 5×10^{-4}. The computations are carried out on a two-dimensional lattice of 200×200

grid points and a constant grid spacing of 0.1. The resulting domain is sufficiently large to avoid undesired perturbations from the system's outer boundaries. The location of the spiral tip is computed from the intersection of space curves with constant u and v (0.26 and 0.1, respectively).

We simulate the interaction of spiral waves with the second type of obstacles, namely heterogeneities of higher excitability (Fig. 7). For this purpose, the parameter ϕ is defined as $\phi_{\mathrm{s}} = \phi$ in the region containing the spiral tip and $\phi_{\mathrm{h}} = \phi + \Delta\phi$ within the heterogeneity. The values of ϕ and $\Delta\phi$ are kept constant at 0.035 and -0.015, respectively. This perturbation is similar to the variations studied by Biktashev et al. for the Barkley model [27]. In Fig. 7(a) we plot the spiral tip trajectory in the presence of a planar heterogeneity. The spiral tip is initially attracted to the obstacle but quickly establishes a drifting motion in the familiar coil-like pattern. As observed in our experiments, the drift velocity is constant for constant $\Delta\phi$. Simulations with different initial conditions confirm the robustness of this effect. Figure 7(b) shows the interaction of a spiral wave with a circular heterogeneity. The spiral tip exhibits a revolving, orbital motion reminiscent of the expected epitrochoidal pattern.

V. CARDIAC SIMULATIONS

An important question is whether the orbital drift can also exist in cardiac systems where the heterogeneity could be caused by anatomical features. While cardiac tissue is an excitable system and hence in the same universality class as the BZ reaction, it does differ in several ways from the chemical reaction-diffusion system. Foremost, wave propagation is not driven by molecular diffusion but by electrical coupling that–in the form of the cable equation–takes a mathematically similar shape. In addition, cardiac tissue shows anisotropic coupling due to fiber rotation within the tissue and systems like the human ventricles are sufficiently thick to require spatially three-dimensional descriptions.

A frequently used model of the human ventricles is the Fenton-Karma model [41, 42]. Although this model considers only a minimal set of variables, it can reproduce the key electrophysiological characteristics of other more complex models [41]. The complete equations

of the model are:

$$\frac{\partial u}{\partial t} = \nabla \cdot (\widetilde{D}\nabla u) - J_{fi}(u;v) - J_{so}(u) - J_{si}(u;w), \tag{2}$$

$$\frac{\partial v}{\partial t} = \Theta(u_c - u)(1-v)/\tau_v^-(u) - \Theta(u-u_c)v/\tau_v^+, \tag{3}$$

$$\frac{\partial w}{\partial t} = \Theta(u_c - u)(1-w)/\tau_w^- - \Theta(u-u_c)w/\tau_w^+. \tag{4}$$

where $\widetilde{D}$ is the diffusion tensor and u, v, and w are the dimensionless membrane potential, a fast ionic gate, and a slow ionic gate, respectively. The gating variables v and w regulate the transmembrane currents. In Eq. 2, J_{fi}, J_{so}, and J_{si} are scaled currents obeying

$$J_{fi}(u;v) = -\frac{v}{\tau_d}\Theta(u-u_c)(1-u)(u-u_c), \tag{5}$$

$$J_{so}(u) = \frac{u}{\tau_o}\Theta(u_c-u) + \frac{1}{\tau_r}\Theta(u-u_c), \tag{6}$$

$$J_{si}(u;w) = -\frac{w}{2\tau_{si}}(1+\tanh[k(u-u_c^{si})]). \tag{7}$$

Here, the values of the parameters are $\tau_v^+ = 3.33$, $\tau_{v1}^- = 19.6$, $\tau_{v1}^- = 1000$, $\tau_w^+ = 667$, $\tau_w^- = 11$, $\tau_d = 0.25 - 0.416$, $\tau_0 = 8.3$, $\tau_r = 50$, $\tau_{si} = 45$, $k = 10$, $u_c^{si} = 0.85$, $u_c = 0.13$, and $u_v = 0.055$. This set of parameters yields a system with negative filament tension [43] but due to the small thickness of the modeled ventricle, linear filaments can remain stable.

The Eq. 2 is integrated by the explicit forward Euler method with a space step of 0.025 cm and a time step of 0.1 ms. The Eqs. 3 and 4 are integrated using the method reported by Rush and Larsen [44] and the same time step of 0.1 s. All simulations are implemented in a square-shaped domain spanning 12.5 cm $\times$ 12.5 cm which for our three-dimensional simulations is extended 1 cm in normal (vertical) direction. Both systems have external no-flux boundaries. The initial condition is either a spiral or a scroll wave with a straight filament extending in the vertical direction. Our simulations are performed using Compute Unified Device Architecture on a NVIDIA (TESLA M2050) graphics processor unit.

Figure 8 shows results of two-dimensional simulations in which the main system had a sodium conductance of $1/\tau_d = 2.4$ but included a central, disk-shaped domain of increased excitability ($1/\tau_d = 4.0$). The black curves are the tip trajectories of single spiral waves positioned near this heterogeneity. In all three simulations Fig. 8(a-c), the diffusion tensor $\widetilde{D}$ is diagonal with a y-component of $D_\parallel = 1.0\ cm^2/s$. The $D_\perp$ component in Fig. 8(a) equals $D_\parallel$ yielding an isotropic medium. In Fig. 8(b, c), however, $D_\perp$ is 5 and 9 times smaller, thus, creating different anisotropic conditions that are more representative of the

actual tissue. Despite the different type of model and the inclusion of anisotropy, we find orbital motion in all three cases. In addition, we observe that the envelope of the trajectory is deformed according to the anisotropy of the system. Perhaps most importantly, these results suggest a robustness of the overall phenomenon.

It is less clear, however, how the effect of orbital motion translates into three dimensions where the heterogeneity could deviate from a simple disk or cylinder. We hence extend our study to three space dimensions considering the example of cone-shaped heterogeneities of increased excitability. Again the sodium conductance is increased within the heterogeneity from 2.4 to 4.0 but only isotropic conditions are studied ($D_{\parallel} = D_{\perp 1} = D_{\perp 2} = 1.0\ cm^2/s$). Figures 9(a,b) show the case of a cylindrical heterogeneity and a cone with a small opening angle of 22 degrees. Note that for the given base radius of 2.5 cm, cones with base angles less than 22 degrees do not span the entire height of the medium and are hence not included in this systematic study. The three-dimensional pattern of the electric potential is illustrated by mapping its distribution in the $z = 0$ plane. The corresponding scroll waves have simple filaments (red lines). The filament in Fig. 9(a) is a straight vertical line, while in Fig. 9(b) it has a slight S-shaped curvature caused by the rigidity of the filament [45] due to interaction with the cone-shaped inhomogeneity. As expected, the filament in Fig. 9(a) describes an orbital motion around the heterogeneity but also the much smaller cone forces the filament to move along its base. The corresponding filament trajectories, as followed at the lower boundary, are shown in Figs. 9(c,d). The curve in Fig. 9(c) is similar to the one in Fig. 8(a) but features a larger number of lobes due to the larger diameter of the cylinder. The trajectory in Fig. 9(d), however, is more complex and reminiscent of meandering. Notice that the curve describes only one rotation around the cone. Accordingly, its intricate structure is the direct result of the cone geometry. Lastly, we investigated the time required for the scroll filament to complete a full rotation around the heterogeneity. For these calculations, the diameter of the cone base is kept constant and the cone base angle is increased from 22 degrees (complete cone) to 90 degrees (cylinder). We observe that the orbital period decreases with decreasing base angle to a value of about 4 s for the cylindrical heterogeneity (Fig. 9(e)). This behavior can be interpreted as an increase in the driving force. Notice that with the exception of the structure with the smallest base angle (22 degrees), all cones in Fig. 9(e) are truncated and span across the entire height of the system.

VI. CONCLUSIONS

Using the photo-sensitive BZ reaction, we have examined the effect of spatial heterogeneities on spiral waves. It is evident that not only the size and shape but also the nature of the heterogeneity strongly affects the dynamics of the spiral tip and hence the characteristics of the global wave pattern. The types of heterogeneities investigated here include impermeable disks and regions that are altered by a reduction of photo-inhibition. These static perturbations cause two interesting responses, namely orbital states and hysteresis. One can speculate that qualitatively different heterogeneities, such as oscillatory or otherwise active regions, can generate a wealth of unexpected phenomena.

The systematic investigation of these phenomena is not only of fundamental interest but can also be motivated by the importance of heterogeneous excitable media in biology. Living cells, tissues, and organs as well as ecological and epidemiological systems are never homogeneous but rather feature a variety of static or time-dependent heterogeneities. An example is the human heart for which anatomical features and traumatic effects, such as infarction, create spatial variations in the tissue parameters. Other examples include social amoebae for which aggregation and cell differentiation cause the formation of developmentally important architectures that are known to affect rotating waves of messenger activity. Clearly one cannot expect to understand such complex living systems by a sole analysis of spatially homogeneous conditions. We therefore complemented our investigations by cardiac simulations that show orbital motion in two-dimensional isotropic and anisotropic media.

The latter examples also raise challenging questions arising from the three-dimensional nature of all biological systems. As shown in our cardiac simulations, the response of excitation waves near heterogeneities carries over into the third space dimension but is complicated by additional degrees of freedom in the filament [46] and the shape of the heterogeneity. For example, for the first time we have shown a filament rigidity [45] caused by the interaction with a cone-shaped inhomogeneity. Beyond the results presented here, we expect that the bistability of pinned and free spiral states should also exist for scroll waves anchored to cylindrical heterogeneities. We suggest that under such conditions, a pinned scroll wave could unpin − in response to a local perturbation − in a front-like fashion. Moreover, one can expect that the filament loop of scroll rings can perform orbital-like motion if perturbed by a nearby torus-shaped heterogeneity. The wealth of dynamic responses in three-dimensional

active systems is immense and clearly requires further investigation.

VII. ACKNOWLEDGEMENTS

E.N., J.F.T., and H.E. thank the German Science Foundation (DFG) for financial support through the Research Training Group 1558 (GRK 1558). E.N. and O.St. acknowledge support by the National Science Foundation under Grant No. 1213259. We thank Ulrike Künkel, Ingeborg Gerdes, and Norbert Zielinski for assistance in the experimental setup and preparation.

VIII. REFERENCES

[1] S. Jakubith, H. H. Rotermund, W. Engel, A. von Oertzen, and G. Ertl, Phys. Rev. Lett. **65**, 3013 (1990).

[2] P. Sadeghi, K. Dunphy, C. Punckt, and H. H. Rotermund, J. Phys. Chem. C **116**, 4686 (2012).

[3] J. M. Davidenko, A. V. Pertsov, R. Salomonsz, W. Baxter, and J. Jalife, Nature (London) **355**, 349 (1992).

[4] S. V. Pandit and J. Jalife, Circ. Res. **112**, 849 (2013).

[5] K. J. Lee, E. C. Cox, and R. E. Goldstein, Phys. Rev. Lett. **76**, 1174 (1996).

[6] A. J. Durston, Proc. Natl. Acad. Sci. USA **110**, 19826 (2013).

[7] E. Pervolaraki and A. V. Holden, Biosystems **112**, 63 (2013).

[8] A. N. Zaikin and A. M. Zhabotinsky, Nature (London) **225**, 535 (1970).

[9] I. R. Epstein, J. A. Pojman, and O. Steinbock, Chaos **16**, 037101 (2006).

[10] O. Steinbock, V. S. Zykov, and S. C. Müller, Nature (London) **366**, 322 (1993).

[11] A. Azhand, J. Totz, and H. Engel, EPL **108**, 10004 (2014).

[12] H. Brandtstädter, M. Braune, I. Schebesch, and H. Engel, Chem. Phys. Lett. **323**, 145 (2000).

[13] O.-U. Kheowan, V. Gáspár, V. S. Zykov, and S. C. Müller, Phys. Chem. Chem. Phys. **3**, 4747 (2001).

[14] S. Grill, V. S. Zykov, and S. C. Müller, Phys. Rev. Lett. **75**, 3368 (1995).

[15] A. L. Lin, M. Bertram, K. Martinez, H. L. Swinney, A. Ardelea, and G. F. Carey, Phys. Rev. Lett. **84**, 4240 (2000).

[16] K. I. Agladze and P. De Kepper, J. Phys. Chem. **96**, 5239 (1992).

[17] A. M. Pertsov and E. A. Ermakova, Biofizica **33**, 338 (1988).

[18] E. A. Ermakova and A. M. Pertsov, Biofizica **31**, 855 (1986).

[19] I. Schebesch and H. Engel, Phys. Rev. E **60**, 6429 (1999).

[20] C. Dupont, K. Agladze, V. Krinsky, Physica A **249** 47 (1998).

[21] Z. A. Jiménez, B. Marts, and O. Steinbock, Phys. Rev. Lett. **102**, 244101 (2009).

[22] E. Nakouzi, Z. A. Jiménez, V. N. Biktashev, and O. Steinbock, Phys. Rev. E **89**, 042902 (2014).

[23] H. Ke, Z. Zhang, and O. Steinbock, J. Phys. Chem. A **118**, 6819 (2014).

[24] H. Ke, Z. Zhang, and O. Steinbock, Phys. Rev. E **91**, 032930 (2015).

[25] S. Alonso, J. Löber, M. Bär, and H. Engel, Eur. Phys. J. Special Topics **187**, 31 (2010).

[26] V. S. Zykov, G. Bordyugov, H. Lentz, and H. Engel, Physica D **239**, 797 (2010).

[27] V. N. Biktashev, D. Barkley, and I. V. Biktasheva, Phys. Rev. Lett. **104**, 058302 (2010).

[28] C. W. Zemlin and A. M. Pertsov, Phys. Rev. Lett. **109**, 038303 (2012).

[29] S. Takagi, A. Pumir, D. Pazó, I. Efimov, V. Nikolski, and V. Krinsky, Phys. Rev. Lett. **93**, 058101 (2004).

[30] Z. Y. Lim, B. Maskara, F. Aguel, R. Jr. Emokpae, and L. Tung, Circulation **114**, 2113 (2006).

[31] A. Isomura, M. Hörning, K. Agladze, and K. Yoshikawa, Phys. Rev. E **78**, 066216 (2008).

[32] R. A. Gray and J. P. Wikswo, Nature (London) **475**, 181 (2011).

[33] X. Feng, X. Gao, D. B. Pan, B. W. Li, and H. Zhang, Sci. Rep. **4**, 4831 (2014).

[34] J. F. Totz, BSc., TU Berlin (2012).

[35] See Supplemental Material at [URL will be inserted by publisher] for a movie of the hysteresis and spiral drift experiments.

[36] O. Steinbock and S. C. Müller, Physica A **188**, 61 (1992).

[37] O. Steinbock, V. S. Zykov, and S. C. Müller, Phys. Rev. E **48**, 3295 (1993).

[38] R. Zhang, L. Yang, A. M. Zhabotinsky, and I. R. Epstein, Phys. Rev. E **76**, 016201 (2007).

[39] H.- J. Krug, L. Pohlmann, and L. Kuhnert, J. Phys. Chem. **94**, 4862 (1990).

[40] R. J. Field, E. Körös, and R. M. Noyes, J. Am. Chem. Soc. **92**, 8649 (1972).

[41] F. Fenton and A. Karma, Chaos **8**, 20 (1998).

[42] F. Fenton, E. M. Cherry, I. Banville, R. A. Gray, H. M. Hastings, A. Karma, and S. J. Evans, Pacing Clin. Electrophysiol. **24**, 538 (2002).

[43] F. Fenton, E. M. Cherry, H. M. Hastings, and S. J. Evans, Chaos **12**, 852 (2002).

[44] S. Rush and H. Larsen, IEEE Trans. Biomed. Eng. **25**, 389 (1978).

[45] H. Dierckx, H. Verschelde, O. Selsil, and V. N. Biktashev, Phys. Rev. Lett. **109**, 174102 (2012).

[46] M. Vinson, A. M. Pertsov, and J. Jalifé, Physica D **72**, 119 (1993).

Figure Captions

FIG. 1 (Color online) Schematic illustration of the experimental setup: (1) observation light source, (2) yellow long-pass filter, (3) condenser lens, (4) flow reactor with BZ reagent, (5) beam splitter, (6) charge-coupled device camera, (7) neutral density filter, (8) blue dichroic filter, (9) controlled light source, (10) computer with LabVIEW platform.

FIG. 2 Still images of spiral waves in the photosensitive BZ system. The patterns are observed in a 0.40 $\pm$ 0.1 mm thick hydrogel matrix containing the immobilized catalyst. A circular disk of 0.65 mm radius is used as an inert and impermeable obstacle. Images show a spiral wave in (a) the pinned state and (b) shortly after unpinning. Image area: 3.3 $\times$ 2.9 cm^2.

FIG. 3 (Color online) (a) Temporal tracking of the spiral tip in a typical hysteresis experiment. The solid, gray circle represents the impermeable disk. The tip trajectory traces the disk circumference in the pinned state (solid, red curve) and evolves into a more expansive curve after unpinning (solid, black circles). Thereafter, the spiral tip traces smaller paths (open, blue circles) before re-establishing the pinned state. (b) Core radius r as a function of applied light intensity P relative to the wavelength of the pinned spiral (λ_p). For a given value of P, r depends on whether the spiral is in the pinned (solid, red circles) or the unpinned state (open, black and blue circles).

FIG. 4. (Color online) Temporal evolution of image brightness (I) at a representative location in the reaction medium. The period T is equivalent to the time lapse between successive peaks and has a constant value when the spiral wave is in the pinned state (solid, red curves). Upon unpinning, T jumps to a large value and then decreases monotonically with decreasing light intensity (dashed, blue curve). The black arrows represent the time points when the light intensity is modified. Finally, the approximate initial period is recovered when the spiral wave returns to the pinned state.

FIG. 5. (Color online) (a) Image of a spiral wave in a reaction medium with non-homogeneous illumination. The dashed, red line represents the border between the bright left region and the right region of 20% lower light intensity.The wavefronts are deformed due to a difference in the propagation velocity between the two regions. (b) The tip trajectory of the spiral wave shows that

the spiral tip drifts parallel to the linear heterogeneity border at a constant velocity. Note that ΔP has a negative value.

FIG. 6 (Color online) (a) Image of a spiral wave in the vicinity of a circular heterogeneity of lower light intensity. (b) The spiral tip attempts an orbital motion, but drifts away because of unintended, weak gradients in the illumination profile. Note that ΔP has a negative value.

FIG. 7 (Color online) Tip trajectories from simulations with ϕ = 0.035 and $\Delta\phi$ = -0.015. The model parameters are provided in the manuscript text. (a) The spiral tip is initially attracted to the heterogeneity boundary which then causes a downward directed steady drift with a constant velocity. (b) The spiral tip undergoes a bi-periodic orbital motion in the presence of a circular heterogeneity.

FIG. 8 (Color online) Two-dimensional cardiac simulations. Spiral tip trajectories (black curves) near a disk-shaped heterogeneity of increased excitability (red border). Within the disk the conductance of sodium ions is increased from 2.4 to 4.0. The three simulations correspond to (a) isotropic and (b,c) anisotropic conditions. The conductivity ratio (vertical-to-horizontal) is 5.0 and 9.0 in (b) and (c), respectively.

FIG. 9 (Color online) Three-dimensional cardiac simulations of scroll wave dynamics near (a,c) a cylindrical and (b,d) a cone-shaped heterogeneity of increased excitability. The red lines in (a,b) are snapshots of the scroll wave filament. The curves in (c,d) are the corresponding trajectories of the filament at the bottom boundary ($z = 0$). (e) Time required to complete a full rotation around the heterogeneity as a function of the cones' base angle. This angle equals 90 and 22 degrees in (a) and (b), respectively.

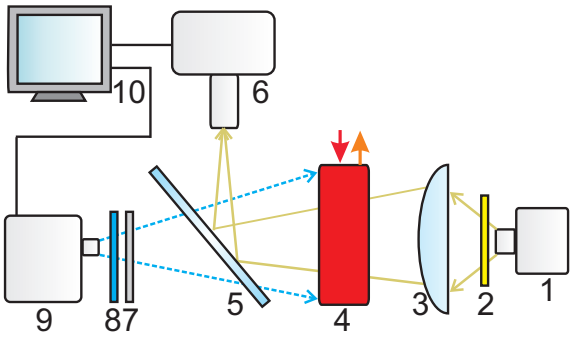

Figure 1

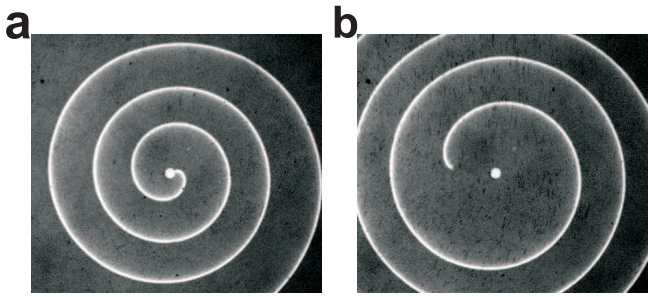

Figure 2

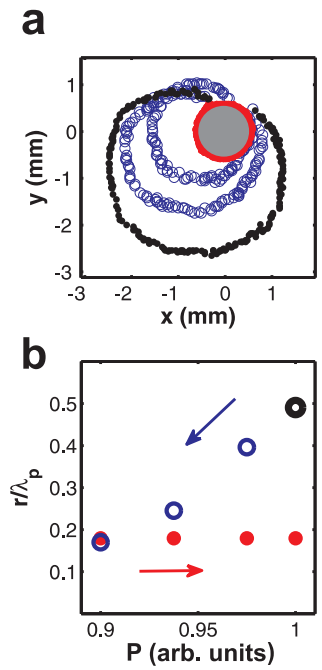

Figure 3

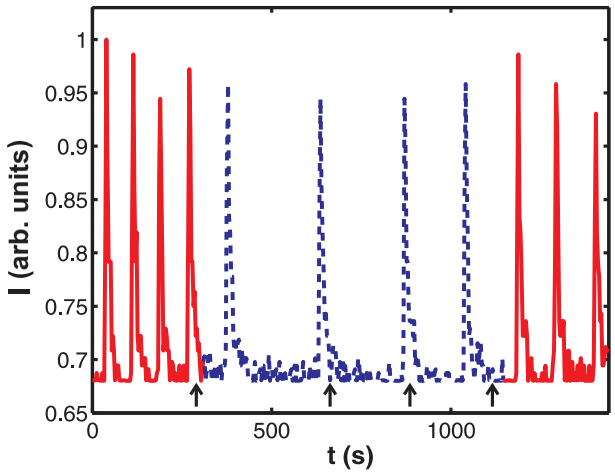

Figure 4

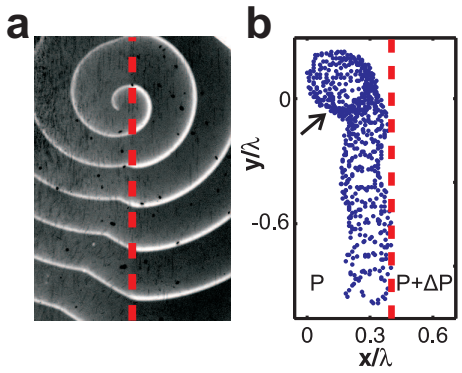

Figure 5

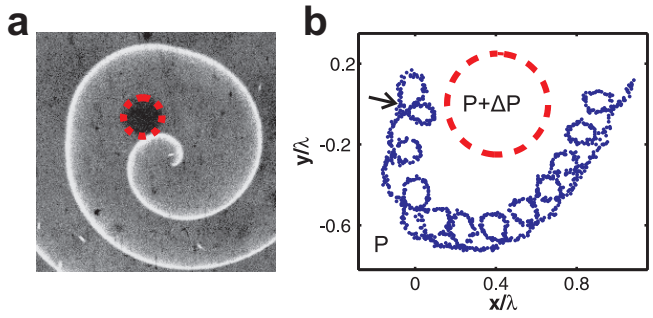

Figure 6

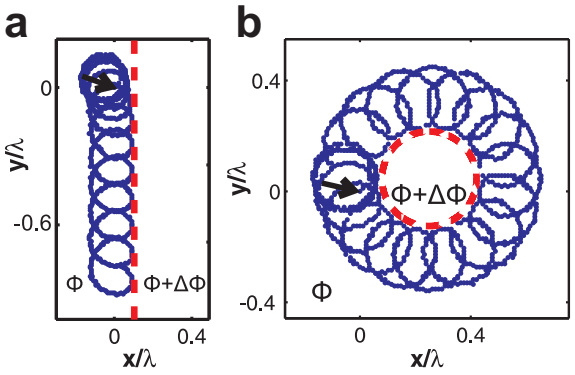

Figure 7

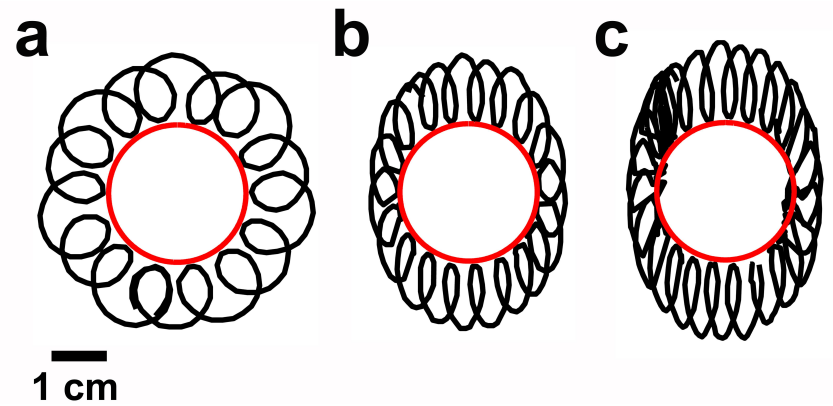

Figure 8

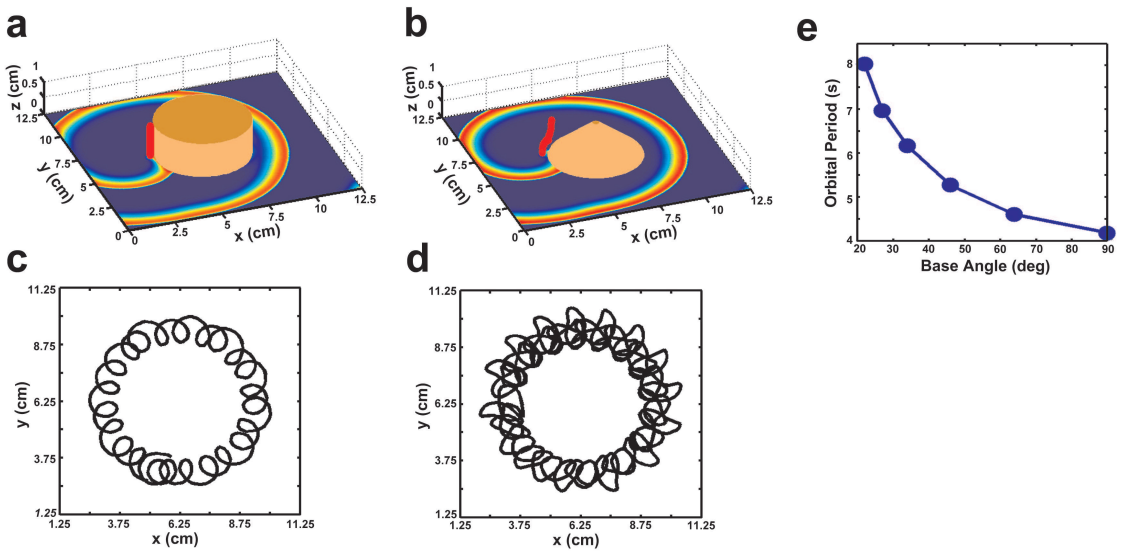

Figure 9